The Multiplexing of Six Vortex Modes in a Multicore Photonic Quasi-Crystal Fiber

Wei Wei, Hongyang Zhao, Yitong Wang, Ziming Dong, Liqin Tang, Lei Ding, and Yigang Li

***Abstract*—We propose a photonic quasi-crystal fiber which has five ring-shaped cores in the cross section. It realizes the multiplexing of 6 vortex modes. The fiber is based on SiO_2 and has an octuple photonic quasi-crystal structure. It achieves four independent dual-core coupling pairs with the optimization of geometric parameters. By adjusting the thickness of five ring-shaped cores, the fundamental mode (HE_{11}) in the small side ring-shaped fiber cores couple to different higher order vector modes (TE_{01}, HE_{21}, TM_{01}, HE_{31}) in the large center ring-shaped fiber core, which makes the light field transfer from small side cores to large center core and realizes the multiplexing of 6 vortex modes (TE_{01}, $OAM^{\pm}_{\pm 1,1}$, TM_{01}, $OAM^{\pm}_{\pm 2,1}$). The transmission characteristics are analyzed with supermode theory. The Δn_{eff} of adjacent vector modes is larger than 10^{-4} due to the thin center ring core. The coupling length (L_c) keeps in the order of 10^{-2} m between 1500–1600 nm and the coupling efficiency is larger than 90% in 1550 nm for four dual-core coupling pairs. We believe this design will have great potential in the field of all-fiber vortex mode division multiplexing.**

***Index Terms*—Fiber communication system, multicore fiber, photonic crystal fiber, vortex mode multiplexing.**

I. Introduction

WITH the rapid development of emerging technologies such as 5G, big data, etc, single mode fiber is approaching capacity limit in recent years. One way to get rid of this crunch is using mode-division multiplexing (MDM) technique to increase the transmission capacity of optical fiber. Different from the traditional multiplexing techniques, mode-division multiplexing technique uses linear polarization modes (LP modes) or vortex modes as the multiplexed channel to transmit signal. LP modes derived from the scalar wave equation without considering refractive index gradient are four-fold degenerate [1]. It will cause inter-mode coupling during long range transmission and increase the complexity of MIMO digital signal processing technique. Nevertheless, vortex modes are obtained by solving the vector wave equation which takes the refractive index gradient into account. They are the vector eigenmodes of cylindrical optical fiber. Vortex modes are divided into polarization vortex modes and phase vortex modes. Polarization vortex modes are also called cylindrical vector modes which contain TE mode and TM mode. Phase vortex modes carrying orbital angular momentum are the OAM modes which have received sustained attention recently [2]. The vortex mode has an annular mode field which has a dark spot in the center. It has a helical phase wavefront represented by $\exp(il\varphi)$, where l is the topological charge number and φ is azimuthal angle [3]. Theoretically, the number of l is infinite and the vortex modes with different l are mutually orthogonal. Compared with fiber supporting LP modes, the fiber supporting vortex modes lifts the inter-mode degeneracy between HE mode and EH mode to the order of 10^{-4} which suppresses the inter-mode crosstalk. So the vortex mode is a good candidate for the MDM technology.

In optical fiber communication system, it is necessary to explore the ways of generation, multiplexing and transmission of vortex modes. So far, researchers have proposed a lot of methods to generate and transmit vortex modes. By using spiral phase plate (SPP) or spatial light modulator (SLM) [4], [5], [6], [7], designing unique fiber structures or optical fiber couplers [8], [9], [10], inscribing bragg gratings in fibers [11], [12], the vortex modes can be generated. The transmission of vortex modes based on the design of ring-shaped fiber, this type of fiber imitates the mode field distribution of vortex mode which has realized the transmission of dozens of vortex modes [13], [14], [15], [16]. Besides the generation and transmission of vortex modes, the multiplexing of vortex modes is a necessary part of the MDM technique. The existing multiplexing techniques mainly based on free-space optical elements in which the purposefully engineered diffractive optical elements can emulate any refractive holographic element to multiplex vortex modes. Such as the cascaded beam splitters [3], photonic integrated circuits [17], SLMs [18], mode sorters [19] and the binary phase Dammann optical vortex gratings [20], [21]. However, the fiber-based multiplexing technique has not been well studied. In order to realize the all-fiber communication of vortex modes, researchers focus on designing fiber-based vortex modes multiplexing element. The preliminary idea is drawing on the design of fiber couplers which utilizes the inter-cores coupling to implement mode conversion. In [22], a fiber based full-vectorial mode generation mechanism was proposed. It realizes the conversion between the fundamental mode (HE_{11}) and higher order full-vectorial mode with coupling mode theory. Later, an all-fiber OAM multiplexer was proposed and realized six OAM modes multiplexing [23]. It uses the back-to-back method and is implemented by the

Manuscript received 29 January 2023; revised 10 March 2023; accepted 13 March 2023. Date of publication 15 March 2023; date of current version 10 April 2023. This work was supported in part by the National Key R&D Program of China under Grant 2020YFB1805800 and in part by the National Natural Science Foundation of China under Grant 12034010. *(Corresponding author: Yigang Li.)*

The authors are with the School of Physics, Nankai University, Tianjin 300071, China (e-mail: nkweiwei@mail.nankai.edu.cn; zhaohongyang@mail.nankai.edu.cn; 2120200243@mail.nankai.edu.cn; 1120210097@mail.nankai.edu.cn; tanya@nankai.edu.cn; dinglei@nankai.edu.cn; liyigang@nankai.edu.cn).

Digital Object Identifier 10.1109/JPHOT.2023.3257503

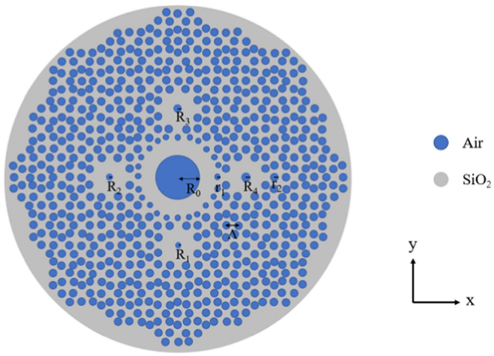

Fig. 1. The cross section of the OPQCF. The geometrical parameters: $R_0 = 3.8\ \mu$m, $R_1 = 0.543\ \mu$m, $R_2 = 0.593\ \mu$m, $R_3 = 0.659\ \mu$m, $R_4 = 0.742\ \mu$m, $r_1 = 0.45\ \mu$m, $r_2 = 0.65\ \mu$m, $\Lambda = 2\ \mu$m.

coupling between conventional graded-index multimode fiber and single mode fibers which have different radius.

Photonic crystal fiber has periodic air hole arrangement which has been studied in-depth by researchers. The unique cross section structure makes it easy to construct fiber couplers [24], [25]. By introducing geometric nonuniformities, a triangular-lattice photonic crystal fiber coupler has been proposed. It can be used as efficient ultrasmall-wavelength splitter or directional coupler for wavelength division multiplexing (WDM) systems [26]. At the same year, Knight et.al theoretically and experimentally demonstrated novel coupling properties in a dual-core all-solid bandgap PCF [27] and Sun Xiwen proposed a novel wavelength-selective coupling PCF which has a highly accurate control of the filtering wavelength [28]. The conventional multi-core fiber mainly uses the fundamental mode to realize the mode coupling and conduct WDM.

In this paper, we propose an octuple photonic quasi-crystal fiber (OPQCF) that realizes the multiplexing of six vortex modes. The substrate of OPQCF is SiO_2. The cross section is featuring with five ring-shaped fiber cores which have different sizes. The thickness of the four small side cores is different which lead to a different effective refractive index (n_{eff}) of fundamental mode. Therefore, the four fundamental modes which have different n_{eff} couple into four different higher-order vortex modes in the center ring-shaped fiber core. The effective refractive index difference (Δn_{eff}) of higher-order vortex modes are larger than 10^{-4} and the design realizes the multiplexing of six vortex modes simultaneously.

II. The Structure of OPQCF

Fig. 1 is the schematic cross section of OPQCF which is designed with the structure of octuple photonic quasi-crystal. The substrate of this design is SiO_2 as shown in the gray part of Fig. 1. The air holes are arranged in the type of octuple photonic quasi-crystal as shown in the blue part of Fig. 1. By removing several rings of air holes in this structure, it forms five ring-shaped fiber cores in the cross section. In order to realize the coupling between HE_{11} mode and higher order vortex modes, the center ring core should have larger core radius to support the transmission of higher order vortex modes. In the design, the center air hole's radius is set to be $R_0 = 3.8\ \mu$m. In addition, the radius of first layer of cladding air holes (r_1) of the center ring core is reduced to $r_1 = 0.45\ \mu$m which increases the coupling efficiency between the corresponding fiber cores. The surrounding four ring cores (core 1, core 2, core 3, core 4) have different center air holes' radius which are $R_1 = 0.543\ \mu$m, $R_2 = 0.593\ \mu$m, $R_3 = 0.659\ \mu$m, $R_4 = 0.742\ \mu$m, respectively. It can meet the phase match between the HE_{11} modes in the four small side cores and the different higher order vortex modes in the large center core. The radius of cladding air holes in the OPQCF is $r_2 = 0.65\ \mu$m and the hole pitch is $\Lambda = 2\ \mu$m.

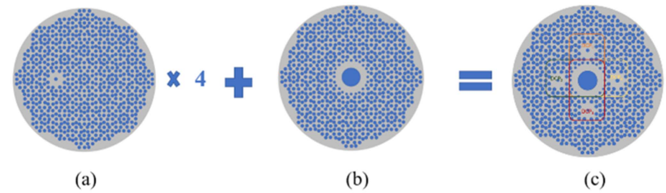

Fig. 2. The design principle of OPQCF. (a) the fiber only with one of the small side cores, (b) the fiber only with the large center core, (c) the final fiber design with four dual-core coupling pairs (DCP_1, DCP_2, DCP_3, DCP_4).

III. The Supermode Theory of OPQCF

The design principle derived from the coupled mode theory in the field of optical fiber. The four small side cores are isolated completely by a lot of air holes as shown in the Fig. 1, so the mode of the four small side cores couples to the large center core independently without coupling to each other. In theorical analysis, this design can be seen as the superposition of four dual-core coupling pairs which are defined as DCP_n where $n = 1{\sim}4$, as shown in the Fig. 2. Each DCP works independently.

According to the coupled mode theory in fiber, in one of the DCP, the interaction between the modes of the two cores satisfies the following equation:

$$\frac{dA_s}{dz} = ik_s A_s + ik_{ls} A_l$$
$$\frac{dA_l}{dz} = ik_l A_l + ik_{ls} A_s \tag{1}$$

In which A_s and A_l are the complex amplitudes of modes in the small side core and the large center core. k_s and k_l are the self-coupling coefficients of modes in each core and k_{ls} is the coupling coefficient between the mode in two cores. The solving process is simplified by expressing the $A_s(z)$ and $A_l(z)$ as $A_s(z) = \tilde{A}_s(z) e^{ik_s z}$ and $A_l(z) = \tilde{A}_l(z) e^{ik_l z}$. Equation (1) is calculated as:

$$\frac{d\tilde{A}_s}{dz} = ik_{ls} \tilde{A}_l e^{i(k_l - k_s)z}$$
$$\frac{d\tilde{A}_l}{dz} = ik_{ls} \tilde{A}_s e^{i(k_s - k_l)z} \tag{2}$$

Express (2) in matrix form:

$$\begin{pmatrix} \tilde{A}'_s \\ \tilde{A}'_l \end{pmatrix} = \begin{pmatrix} 0 & ik_{ls} e^{i(k_l - k_s)z} \\ ik_{ls} e^{i(k_s - k_l)z} & 0 \end{pmatrix} \begin{pmatrix} \tilde{A}_s \\ \tilde{A}_l \end{pmatrix} \tag{3}$$

Equation (3) can be solved as:

$$\begin{pmatrix} \tilde{A}_s \\ \tilde{A}_l \end{pmatrix} = c_1 \begin{pmatrix} 1 \\ e^{i(k_s - k_l)z} \end{pmatrix} e^{ik_{ls}z} + c_2 \begin{pmatrix} 1 \\ -e^{i(k_s - k_l)z} \end{pmatrix} e^{-ik_{ls}z} \tag{4}$$

Substitute (4) into $A_s\ (z) = \tilde{A}_s\ (z) e^{ik_s z}$ and $A_l\ (z) = \tilde{A}_l\ (z) e^{ik_l z}$ and get:

$$\begin{pmatrix} A_s \\ A_l \end{pmatrix} = \begin{pmatrix} \tilde{A}_s e^{ik_s z} \\ \tilde{A}_l e^{ik_l z} \end{pmatrix} = c_1 \begin{pmatrix} 1 \\ 1 \end{pmatrix} e^{i(k_{ls} + k_s)z} + c_2 \begin{pmatrix} 1 \\ -1 \end{pmatrix} e^{i(k_s - k_{ls})z} \tag{5}$$

If it is assumed that the light is launched into the small side core with fundamental mode at $z = 0$, the initial condition can be expressed as $A_s\ (0) = A_0$ and $A_l\ (0) = 0$. Substituting this condition into (5), we get $c_1 = c_2 = A_0/2$. In the end, the solution of (1) is:

$$\begin{pmatrix} A_s \\ A_l \end{pmatrix} = \frac{A_0}{2} \begin{pmatrix} 1 \\ 1 \end{pmatrix} e^{i(k_s + k_{ls})z} + \frac{A_0}{2} \begin{pmatrix} 1 \\ -1 \end{pmatrix} e^{i(k_s - k_{ls})z} \tag{6}$$

Therefore, when the dual-core waveguide is considered as a whole, the dual-core coupling can be viewed as the superposition of two modes with two different propagation constants. These modes are defined as supermodes. According to (6), the complex amplitude of the two supermodes are:

$$A_1 = \frac{A_0}{2} \begin{pmatrix} 1 \\ 1 \end{pmatrix} e^{i(k_s + k_{ls})z}, A_2 = \frac{A_0}{2} \begin{pmatrix} 1 \\ -1 \end{pmatrix} e^{i(k_s - k_{ls})z} \tag{7}$$

In which A_1 and A_2 are the complex amplitudes of supermodes. In order to realize the dual-core efficient mode coupling, the modes in the two cores should satisfy the phase match condition and have the same propagation constants. Substituting (7) into the electric field expression:

$$\boldsymbol{E}(r, \varphi, z) = A(z) F(r) \Phi(\varphi) e^{i\beta z} \tag{8}$$

And we get:

$$\boldsymbol{E}_1(r, \varphi, z) = \frac{A_0}{2} \begin{pmatrix} 1 \\ 1 \end{pmatrix} F(r)_1 \Phi(\varphi)_1 e^{i(\beta + k_s + k_{ls})z}$$
$$\boldsymbol{E}_2(r, \varphi, z) = \frac{A_0}{2} \begin{pmatrix} 1 \\ -1 \end{pmatrix} F(r)_2 \Phi(\varphi)_2 e^{i(\beta + k_s - k_{ls})z} \tag{9}$$

The electric field of two supermodes have different propagation constant which are $\beta + k_s + k_{ls}$ and $\beta + k_s - k_{ls}$, respectively. The two supermodes have symmetric and antisymmetric distributed amplitudes which are $(11)'$ and $(1\ -1)'$, respectively. So, one of the fiber cores has the same amplitude distribution, and the other core has inverse amplitude distribution. The total electric field is expressed as:

$$E = \frac{A_0}{2} \begin{pmatrix} 1 \\ 1 \end{pmatrix} F(r)_1 \Phi(\varphi)_1 e^{i(\beta + k_s + k_{ls})z} + \frac{A_0}{2} \begin{pmatrix} 1 \\ -1 \end{pmatrix} F(r)_2 \Phi(\varphi)_2 e^{i(\beta + k_s - k_{ls})z} \tag{10}$$

IV. Numerical Result With Supermode Theory

Finite element method (FEM) regards the dual-core waveguide as a whole and can work out the supermodes of waveguide. The supermodes are defined as SM_n in the design, where n is positive integer. Fig. 3 represents the mode field distribution of supermods calculated with FEM at 1550 nm. The four small side cores are decoupled because of the isolation of air holes. For the DCP_1, the mode field distribution of two supermodes are SM_1 and SM_2 as shown in Fig. 3. The HE_{11}^x in the core 1 and the TE_{01} in the large center core can meet the phase match condition and realize efficient coupling. The two supermodes have different n_{eff} which are n_{even} and n_{odd}, respectively. The supermode which effective refractive index is n_{even} corresponds to the symmetric distributed amplitudes and the n_{odd} corresponds to the antisymmetric distributed amplitudes. At the initial state, we input the HE_{11}^x to the core 1, after a coupling length (L_c), the two supermodes have a phase difference of π, the light field will move to the large center core because of the coupling effect. The expression of the coupling length is as follows [26]:

$$L_c = \frac{\pi}{|\beta_{even} - \beta_{odd}|} = \frac{\lambda}{2|n_{even} - n_{odd}|} \tag{11}$$

In which $\beta_{even} = \ \beta + k_s + k_{ls}$ and $\beta_{odd} = \ \beta + k_s - k_{ls}$. They are propagation constants of the supermodes.

For the DCP_2 it realizes the coupling between HE_{11} in core 2 and HE_{21} mode in large center core. The corresponding modes are SM_3 to SM_6. Different from the core 1. In the core 2, the HE_{11}^x coupling to $\text{HE}_{21}^{\text{even}}$ which corresponds to SM_3 and SM_4, the HE_{11}^y coupling to $\text{HE}_{21}^{\text{odd}}$ which corresponds to SM_5 and SM_6. When we input $\text{HE}_{11}^x + \text{HE}_{11}^y$ to the core 2, it will couple to the large center core with mode $\text{HE}_{21}^{even} + i\text{HE}_{21}^{odd}$, which change the fundamental mode to one-order phase vortex mode ($\text{OAM}_{\pm 11}^{\pm}$). Based on the same principle, the DCP_3 realizes the coupling between the HE_{11}^y in the core 3 and the TM_{01} in the large center core, the corresponding supermodes are SM_7 and SM_8. The DCP_4 realizes the coupling between HE_{11} in the core 4 and $\text{OAM}_{\pm 21}^{\pm}$ mode in the large center core. The four supermodes are SM_9 to SM_{12}. This design realizes the coupling between fundamental modes and vortex modes.

Fig. 4 shows the 3D electric field of supermodes (HE_{11}^y coupling to HE_{21}^{odd}) calculated with the FEM at 1550 nm. For the two supermodes, the HE_{11}^y mode in the core 2 has inverse electric field, the HE_{21}^{odd} mode in the large center core has same electric field. It is consistent with the theoretical derivation. In Fig. 5, we present the 2D electric field of all supermodes, each pair of supermodes has a consistent mode field distribution.

In order to realize non-crosstalk multiplexing of vortex modes, the Δn_{eff} of adjacent vector modes should be larger than 10^{-4}. Fig. 6 represents the Δn_{eff} of adjacent vector mode supported in the large center core as shown in Fig. 2(b). In 1000 - 2000 nm, the large center core supports 8 vector modes' transmission, corresponding to 12 vortex modes (TE_{01}, TM_{01}, $\text{OAM}_{\pm 11}^{\pm}$, $\text{OAM}_{\pm 21}^{\pm}$, $\text{OAM}_{\pm 21}^{\mp}$, $\text{OAM}_{\pm 31}^{\pm}$, $\text{OAM}_{\pm 31}^{\mp}$). In the range of 1200–2000 nm, the Δn_{eff} of all adjacent vector modes are larger than 10^{-4} which promises the efficient multiplexing of vortex modes. In the design, we couple the fundamental mode

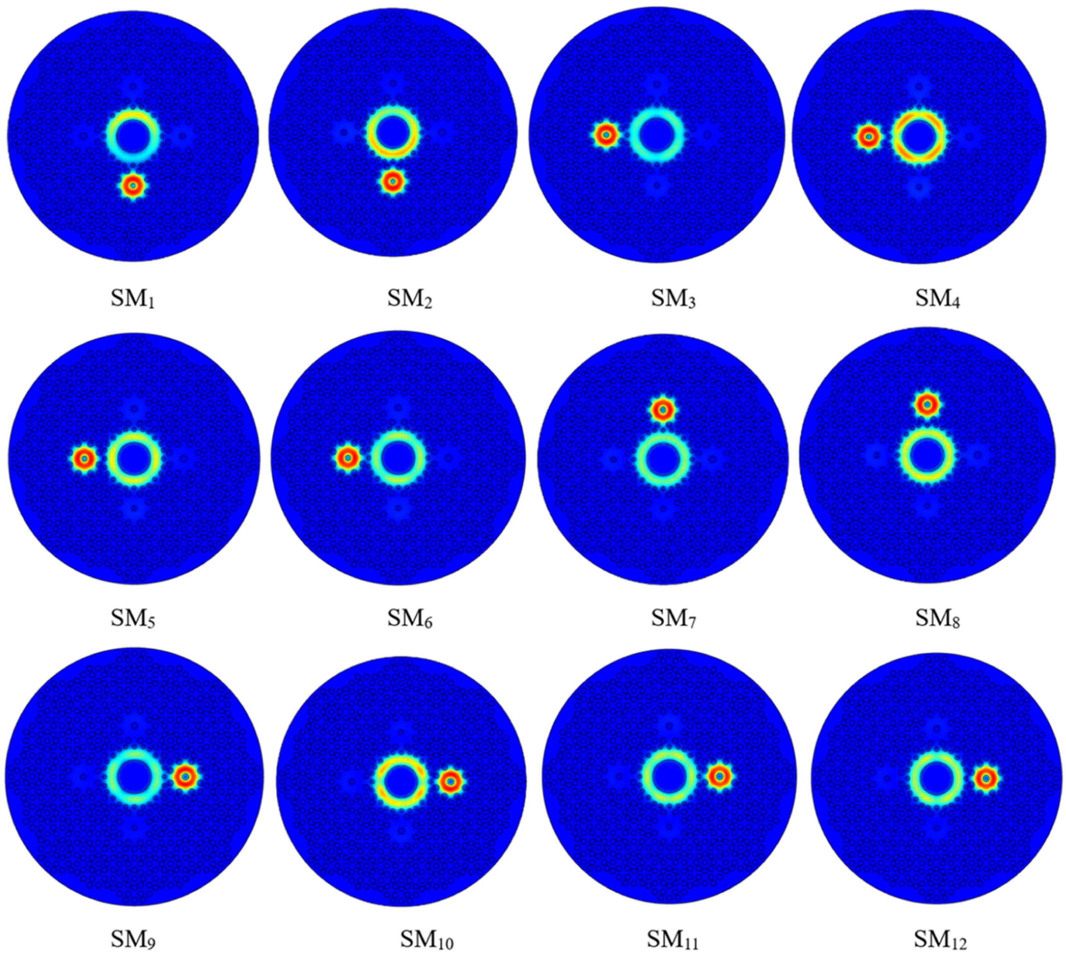

Fig. 3. The mode field distribution of supermodes calculated with the finite element method at 1550 nm.

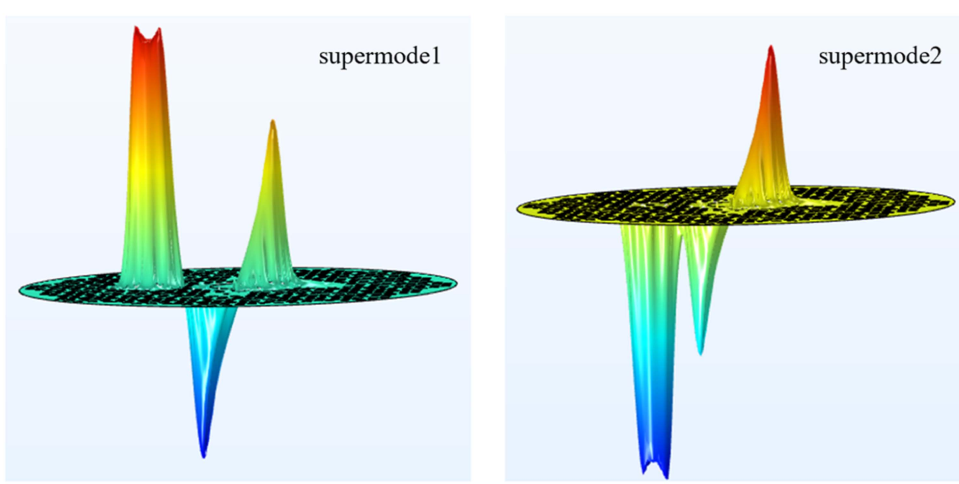

Fig. 4. The 3D electric field of supermodes (HE_{11}^{y} coupling to HE_{21}^{odd}) calculated with the FEM at 1550 nm.

into the first and second order vortex modes without use the third order vortex modes. So, we focus on the first and second order vortex modes in the later research.

Fig. 7 represents the n_{eff} of vector modes in the large center core and HE_{11} modes in four small side cores with the change of wavelength. In Fig. 7(a), the n_{eff} of vector modes in the large center core and HE_{11} modes in the four small side cores decrease with wavelength and the slop of vector modes in the large center core are larger than that of HE_{11} modes. Because of the different radius of small side cores, the n_{eff} of HE_{11} modes

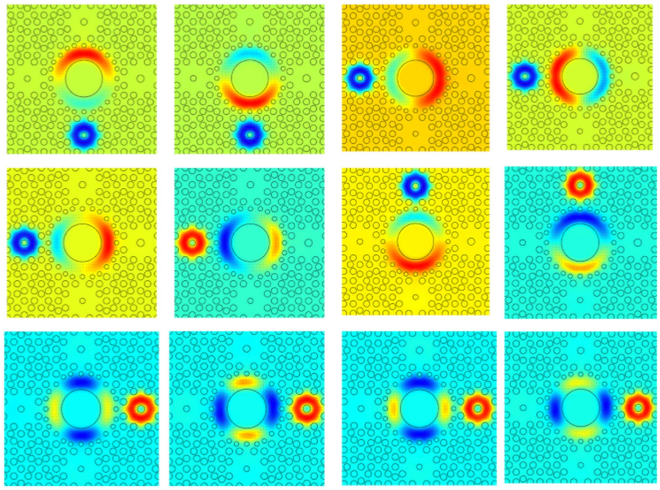

Fig. 5. The 2D electric field of all supermodes calculated with FEM at 1550 nm.

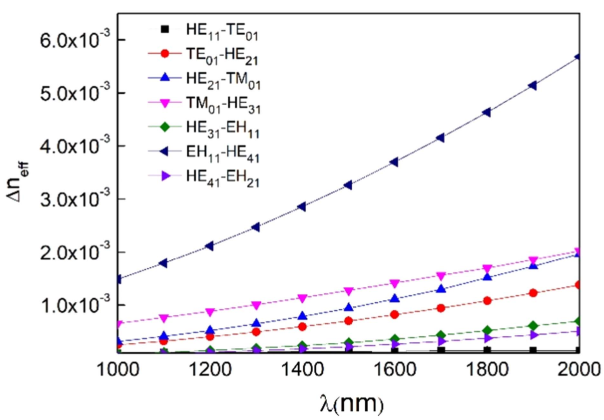

Fig. 6. The Δn_{eff} of adjacent vector mode supported in the large center core as shown in Fig. 2(b) with the change of wavelength.

overlap with the n_{eff} of different higher order vector modes at different wavelength range, respectively. In the overlapping wavelength range, it realizes inter-mode coupling, and the HE_{11} mode can be coupled into higher order vector modes over a relatively long wavelength range, but with different coupling efficiency. We change the radius of four small side cores and adjust the overlap waveband to 1550 nm as shown in Fig. 7(b). The coupling efficiency can be highest at 1550 nm. The final optimized radius of four small side cores is $R_1 = 0.543$ μm, $R_2 = 0.593$ μm, $R_3 = 0.659$ μm, $R_4 = 0.742$ μm, respectively.

Fig. 8(a) shows the L_c of the four independent dual-core coupling with the change of wavelength. In Fig. 8(a), the L_c keeps in the order of 10^{-2} m in the range of 1500–1600 nm. In 1550 nm, the L_c for the supermode of four DCP are 1.67 cm, 1.45 cm, 1.21 cm and 1.36 cm, respectively, which guarantees an integrated fiber design. Fig. 8(b) presents the coupling efficiency of the four independent DCP with the change of wavelength. We define the coupling efficiency as $\min(Power_{even}, Power_{odd})/\max(Power_{even}, Power_{odd})$, in which the $Power_{even}$ represents the power of even supermode and the $Power_{odd}$ represents the power of odd supermode. The

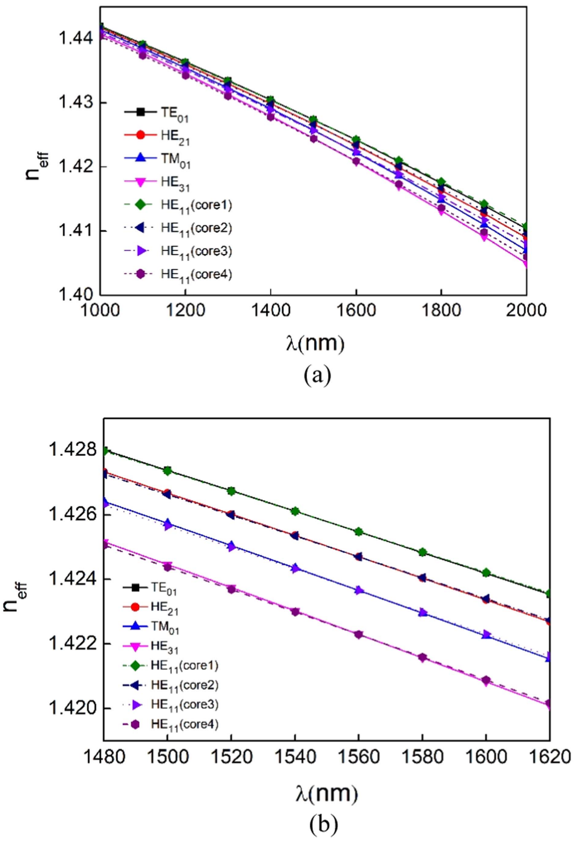

Fig. 7. (a) The n_{eff} of vector mode supported in the large center core and the n_{eff} of HE_{11} mode in four small side cores between 1000–2000 nm, (b) the detail of (a) between 1480–1620 nm.

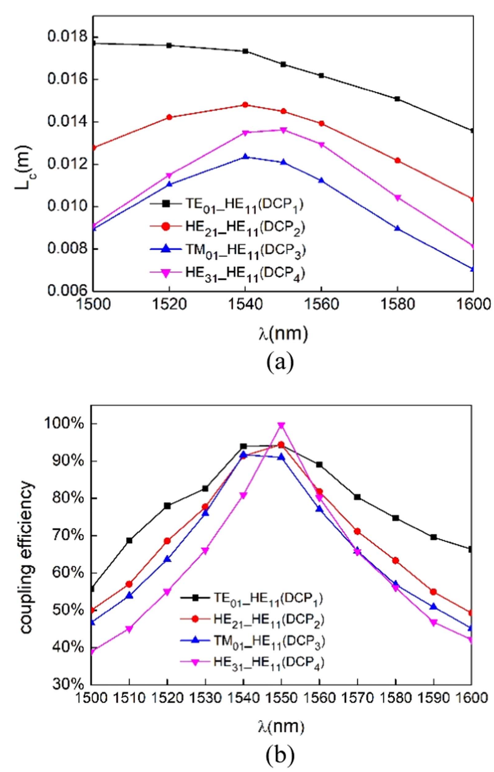

Fig. 8. (a) The L_c and (b) the coupling efficiency of four independent DCP with the change of wavelength.

coupling bandwidth decreases with the order of vector modes, in which the DCP_1 has the maximum bandwidth and the DCP_4 has the minimum bandwidth. By adjusting fiber structure, the four DCPs realize the optimal coupling efficiency in 1550 nm which are larger than 90%. The biggest coupling efficiency is 99.8% for the DCP_4 in 1550 nm.

V. Conclusion

In this paper, we propose a photonic quasi-crystal fiber supporting the multiplexing of six vortex modes. It provides a new idea for all-fiber vortex mode multiplexing. The PCF is based on SiO_2 and design with the octuple photonic quasi-crystal structure. The design contains five ring-shaped cores in the cross section and realizes four independent dual-core coupling. The four small side cores setting with different thickness make HE_{11} mode couple into different higher order vortex modes (TE_{01}, $OAM^{\pm}_{\pm 11}$, TM_{01}, $OAM^{\pm}_{\pm 21}$) in the large center cores. By simulation, the adjacent vector modes' is larger than 10^{-4}, which suppresses the mode crosstalk in the large center core. Analyzing with supermode theory, the L_c of four pairs of supermodes are in the order of 10^{-2} m and the coupling efficiency are larger than 90% in 1550 nm. In the future design, we can change the geometrical parameters of the design to realize the phase match between fundamental mode and higher order vector modes with larger *l* and make the multiplexing of higher order vortex modes possible.

In our design, the precision of the air hole' radii is really important. The air hole's accuracy relies on the improvement of photonic crystal fiber manufacturing technology. As far as we know, the manufacture of photonic crystal fiber has reached a high precision. In [29], the control accuracy over PCF's air hole radius has reached the order of nanometer. Therefore, we believe that the manufacture technologies are mature enough for the OPQCF we designed.

References

[1] C. Brunet and L. A. Rusch, "Optical fibers for the transmission of orbital angular momentum modes," *Opt. Fiber Technol.*, vol. 35, pp. 2–7, Feb. 2017, doi: 10.1016/j.yofte.2016.09.016.

[2] S. Ramachandran and P. Kristensen, "Optical vortices in fiber," *Nanophoton.*, vol. 2, no. 5–6, pp. 455–474, Dec. 2013, doi: 10.1515/nanoph-2013-0047.

[3] A. E. Willner et al., "Optical communications using orbital angular momentum beams," *Adv. Opt. Photon.*, vol. 7, no. 1, pp. 66–106, Mar. 2015, doi: 10.1364/AOP.7.000066.

[4] W. Harm, S. Bernet, M. Ritsch-Marte, I. Harder, and N. Lindlein, "Adjustable diffractive spiral phase plates," *Opt. Exp.*, vol. 23, no. 1, pp. 413–421, Jan. 2015, doi: 10.1364/OE.23.000413.

[5] Z. Guo et al., "Fabrication of spiral phase plate using photoresist for OAM generation," in *Proc. Asia Commun. Photon. Conf.*, 2019, pp. 1–3.

[6] S. Li and J. Wang, "Adaptive power-controllable orbital angular momentum (OAM) multicasting," *Sci. Rep.*, vol. 5, no. 1, May 2015, Art. no. 9677, doi: 10.1038/srep09677.

[7] F. Zhu et al., "Free-space optical communication link using perfect vortex beams carrying orbital angular momentum (OAM)," *Opt. Commun.*, vol. 396, pp. 50–57, Aug. 2017, doi: 10.1016/j.optcom.2017.03.023.

[8] G. Wong et al., "Excitation of orbital angular momentum resonances in helically twisted photonic crystal fiber," *Sci.*, vol. 337, pp. 446–449, Jul. 2012, doi: 10.1126/science.1223824.

[9] C. Zhao et al., "Design of multicore photonic crystal fibers to generate cylindrical vector beams," *J. Lightw. Technol.*, vol. 34, no. 4, pp. 1206–1211, Feb. 2016.

[10] Y. Yan et al., "Efficient generation and multiplexing of optical orbital angular momentum modes in a ring fiber by using multiple coherent inputs," *Opt. Lett.*, vol. 37, no. 17, pp. 3645–3647, Sep. 2012, doi: 10.1364/OL.37.003645.

[11] Y. Zhao, Y. Liu, L. Zhang, C. Zhang, J. Wen, and T. Wang, "Mode converter based on the long-period fiber gratings written in the two-mode fiber," *Opt. Exp.*, vol. 24, no. 6, pp. 6186–6195, Mar. 2016, doi: 10.1364/OE.24.006186.

[12] X. Zhang, A. Wang, R. Chen, Y. Zhou, H. Ming, and Q. Zhan, "Generation and conversion of higher order optical vortices in optical fiber with helical fiber Bragg gratings," *J. Lightw. Technol.*, vol. 34, no. 10, pp. 2413–2418, May 2016.

[13] C. Brunet, P. Vaity, Y. Messaddeq, S. LaRochelle, and L. A. Rusch, "Design, fabrication and validation of an OAM fiber supporting 36 states," *Opt. Exp.*, vol. 22, no. 21, pp. 26117–26127, Oct. 2014, doi: 10.1364/OE.22.026117.

[14] N. Bozinovic et al., "Terabit-scale orbital angular momentum mode division multiplexing in fibers," *Sci.*, vol. 340, no. 6140, pp. 1545–1548, Jun. 2013, doi: 10.1126/science.1237861.

[15] A. Tandjè et al., "Ring-core photonic crystal fiber for propagation of OAM modes," *Opt. Lett.*, vol. 44, no. 7, pp. 1611–1614, Apr. 2019, doi: 10.1364/OL.44.001611.

[16] W. Wei, N. An, Z. Zhang, L. Tang, L. Ding, and Y. Li, "Design of a microstructure optical fiber supporting 52 vortex beams," *Opt. Commun.*, vol. 490, Jul. 2021, Art. no. 126657, doi: 10.1016/j.optcom.2020.126657.

[17] N. K. Fontaine, C. R. Doerr, and L. L. Buhl, "Efficient multiplexing and demultiplexing of free-space orbital angular momentum using photonic integrated circuits," in *Proc. Opt. Fiber Commun. Conf.*, 2012, pp. 1–3, doi: 10.1364/OFC.2012.OTu1I.2.

[18] Y. Yan et al., "Multicasting in a spatial division multiplexing system based on optical orbital angular momentum," *Opt. Lett.*, vol. 38, no. 19, pp. 3930–3933, Oct. 2013, doi: 10.1364/OL.38.003930.

[19] H. Huang et al., "Tunable orbital angular momentum mode filter based on optical geometric transformation," *Opt. Lett.*, vol. 39, no. 6, pp. 1689–1692, Mar. 2014, doi: 10.1364/OL.39.001689.

[20] T. Lei et al., "Massive individual orbital angular momentum channels for multiplexing enabled by Dammann gratings," *Light: Sci. Appl.*, vol. 4, no. 3, Mar. 2015, Art. no. e257, doi: 10.1038/lsa.2015.30.

[21] N. Zhang, X. C. Yuan, and R. E. Burge, "Extending the detection range of optical vortices by Dammann vortex gratings," *Opt. Lett.*, vol. 35, no. 20, pp. 3495–3497, Oct. 2010, doi: 10.1364/OL.35.003495.

[22] L. Fang and J. Wang, "Full-vectorial mode coupling in optical fibers," *IEEE J. Quantum Electron.*, vol. 54, no. 2, Apr. 2018, Art. no. 6800207, doi: 10.1109/JQE.2018.2810326.

[23] W. Zhou, H. Cao, L. Wang, and J. Wang, "All-fiber orbital angular momentum (OAM) functional devices for mode-division (de) multiplexing in conventional graded-index multimode fiber," in *Proc. Opt. Fiber Commun. Conf. Exhib.*, 2019, pp. 1–3, doi: 10.1364/OFC.2019.Th3D.5.

[24] F. Fogli, L. Saccomandi, P. Bassi, G. Bellanca, and S. Trillo, "Full vectorial BPM modeling of index-guiding photonic crystal fibers and couplers," *Opt. Exp.*, vol. 10, no. 1, pp. 54–59, Jan. 2002, doi: 10.1364/OE.10.000054.

[25] N. Mothe and P. D. Bin, "Numerical analysis of directional coupling in dual-core microstructured optical fibers," *Opt. Exp.*, vol. 17, no. 18, pp. 15778–15789, Aug. 2009, doi: 10.1364/OE.17.015778.

[26] M. Zghal, R. Cherif, and F. Bahloul, "Improving triangular-lattice photonic-crystal-fiber couplers by introducing geometric nonuniformities," *Opt. Eng.*, vol. 46, no. 9, Sep. 2007, Art. no. 095004, doi: 10.1117/1.2783388.

[27] Z. Wang, T. Taru, T. A. Birks, J. C. Knight, Y. Liu, and J. Du, "Coupling in dual-core photonic bandgap fibers: Theory and experiment," *Opt. Exp.*, vol. 15, no. 8, pp. 4795–4803, Apr. 2007, doi: 10.1364/OE.15.004795.

[28] X. Sun, "Wavelength-selective coupling of dual-core photonic crystal fiber with a hybrid light-guiding mechanism," *Opt. Lett.*, vol. 32, no. 17, pp. 2484–2486, Sep. 2007, doi: 10.1364/OL.32.002484.

[29] X. Zhang, Y. Liu, Z. Wang, J. Yu, and H. Zhang, "LP_{01}-LP_{11a} mode converters based on long-period fiber gratings in a two-mode polarization-maintaining photonic crystal fiber," *Opt. Exp.*, vol. 26, no. 6, pp. 7013–7021, Mar. 2018, doi: 10.1364/OE.26.007013.